Generation of femtosecond optical vortices by molecular modulation in a Raman-active crystal

Miaochan Zhi, Kai Wang, Xia Hua, Hans Schuessler, James Strohaber, and Alexei V. Sokolov*

Institute for Quantum Science and Engineering, Department of Physics and Astronomy, Texas A&M University, College Station, Texas 77843-4242, USA

**sokol@physics.tamu.edu*

Abstract: We have generated multi-color optical vortices in a Raman-active crystal $PbWO_4$ using two-color Fourier-transform limited femtosecond laser pulses. This setup overcomes some of the limitation of our previous research by allowing for the production of subcycle femtosecond optical vortices without the need for compensating for added chirp. In addition, the use of an OPA allows for greater flexibility in exciting different Raman modes. We verified the topological charges using two different methods. These diagnostic experiments verify not only theoretically predicted OAM algebra but demonstrated instabilities in high-order OVs. We have also studied factors which affect the high-order vortex sidebands such as the diameter and intensity of the input beams.

OCIS codes: (190.7110) Ultrafast nonlinear optics; (050.4865) Optical vortices.

References and links

1. A. M. Yao and M. J. Padgett, "Orbital angular momentum: origins, behavior and applications," Adv. Opt. Photon. **3**(2), 161–204 (2011).
2. F. M. Fazal and S. M. Block, "Optical tweezers study life under tension," Nat. Photonics **5**(6), 318–321 (2011).
3. A. Yu. Okulov, "Cold matter trapping via slowly rotating helical potential," Phys. Lett. A **376**(4), 650–655 (2012).
4. B. Neupane, F. Chen, W. Sun, D. T. Chiu, and G. F. Wang, "Tuning donut profile for spatial resolution in stimulated emission depletion microscopy," Rev. Sci. Instrum. **84**(4), 043701–043709 (2013).
5. G. R. M. Robb, "Superradiant exchange of orbital angular momentum between light and cold atoms," Phys. Rev. A **85**(2), 023426 (2012).
6. M. J. Padgett, "Light in a twist: optical angular momentum," Proc. SPIE **8637**, 863702, 863702-10 (2013).
7. C. Hnatovsky, V. G. Shvedov, W. Krolikowski, and A. V. Rode, "Materials processing with a tightly focused femtosecond laser vortex pulse," Opt. Lett. **35**(20), 3417–3419 (2010).
8. K. Toyoda, K. Miyamoto, N. Aoki, R. Morita, and T. Omatsu, "Using Optical Vortex To Control the Chirality of Twisted Metal Nanostructures," Nano Lett. **12**(7), 3645–3649 (2012).
9. M. Vasnetsov and K. Staliunas, eds., Optical Vortices (Nova Science Publishers, Inc.) Chapter **8**. "Interaction of optical vortices in nonlinear crystals" (1999).
10. T. Yusufu, Y. Tokizane, M. Yamada, K. Miyamoto, and T. Omatsu, "Tunable 2-μm optical vortex parametric oscillator," Opt. Express **20**(21), 23666–23675 (2012).
11. F. Lenzini, S. Residori, F. T. Arecchi, and U. Bortolozzo, "Optical vortex interaction and generation via nonlinear wave mixing," Phys. Rev. A **84**(6), 061801 (2011).
12. K. Dholakia, N. B. Simpson, M. J. Padgett, and L. Allen, "Second-harmonic generation and the orbital angular momentum of light," Phys. Rev. A **54**(5), R3742–R3745 (1996).
13. F. A. Bovino, M. Braccini, M. Giardina, and C. Sibilia, "Orbital angular momentum in noncollinear second-harmonic generation by off-axis vortex beams," J. Opt. Soc. Am. B **28**(11), 2806–2811 (2011).
14. K. Bezuhanov, A. Dreischuh, G. G. Paulus, M. G. Schätzel, and H. Walther, "Vortices in femtosecond laser fields," Opt. Lett. **29**(16), 1942–1944 (2004).
15. I. Mariyenko, J. Strohaber, and C. Uiterwaal, "Creation of optical vortices in femtosecond pulses," Opt. Express **13**(19), 7599–7608 (2005).

#193113 - $15.00 USD Received 1 Jul 2013; revised 5 Sep 2013; accepted 9 Sep 2013; published 5 Nov 2013

16. J. Strohaber, C. Petersen, and C. J. G. J. Uiterwaal, "Efficient angular dispersion compensation in holographic generation of intense ultrashort paraxial beam modes," Opt. Lett. **32**(16), 2387–2389 (2007).
17. M. Zhi and A. V. Sokolov, "Toward single-cycle pulse generation in Raman-active crystals," IEEE Journal of Selected Topics in Quantum Electronics on Ultrafast Science and Technology **18**(1), 460–466 (2012).
18. H. S. Chan, Z. M. Hsieh, W. H. Liang, A. H. Kung, C. K. Lee, C. J. Lai, R. P. Pan, and L. H. Peng, "Synthesis and Measurement of Ultrafast Waveforms from Five Discrete Optical Harmonics," Science **331**(6021), 1165–1168 (2011).
19. A. V. Sokolov, M. Y. Shverdin, D. R. Walker, D. D. Yavuz, A. M. Burzo, G. Y. Yin, and S. E. Harris, "Generation and control of femtosecond pulses by molecular modulation," J. Mod. Opt. **52**, 285–304 (2005).
20. J. Strohaber, M. Zhi, A. V. Sokolov, A. A. Kolomenskii, G. G. Paulus, and H. A. Schuessler, "Coherent transfer of optical orbital angular momentum in multi-order Raman sideband generation," Opt. Lett. **37**(16), 3411–3413 (2012).
21. M. Zhi, K. Wang, X. Hua, and A. V. Sokolov, "Pulse-shaper-assisted phase control of a coherent broadband spectrum of Raman sidebands," Opt. Lett. **36**(20), 4032–4034 (2011).
22. A. V. Gorbach, D. V. Skryabin, and C. N. Harvey, "Vortex solitons in an off-resonant Raman medium," Phys. Rev. A **77**(6), 063810 (2008).
23. M. Zhi, K. Wang, and A. V. Sokolov, "Toward single-cycle pulse generation in single-crystal diamond," 17th International conference on ultrafast phenomena, Snowmass, Colorado (2010).
24. S. S. R. Oemrawsingh, J. A. W. van Houwelingen, E. R. Eliel, J. P. Woerdman, E. J. K. Verstegen, J. G. Kloosterboer, and G. W. 't Hooft, "Production and Characterization of Spiral Phase Plates for Optical Wavelengths," Appl. Opt. **43**(3), 688–694 (2004).
25. M. C. Zhi, X. Wang, and A. V. Sokolov, "Broadband coherent light generation in diamond driven by femtosecond pulses," Opt. Express **16**(16), 12139–12147 (2008).
26. C.-S. Guo, L.-L. Lu, and H.-T. Wang, "Characterizing topological charge of optical vortices by using an annular aperture," Opt. Lett. **34**(23), 3686–3688 (2009).
27. M. E. Anderson, H. Bigman, L. E. E. de Araujo, and J. L. Chaloupka, "Measuring the topological charge of ultrabroadband, optical-vortex beams with a triangular aperture," J. Opt. Soc. Am. B **29**(8), 1968–1976 (2012).
28. P. Vaity, J. Banerji, and R. P. Singh, "Measuring the topological charge of an optical vortex by using a tilted convex lens," Phys. Lett. A **377**(15), 1154–1156 (2013).
29. F. Ricci, W. Löffler, and M. P. van Exter, "Instability of higher-order optical vortices analyzed with a multi-pinhole interferometer," Opt. Express **20**(20), 22961–22975 (2012).

1. Introduction

Optical vortices (OVs) are beams of light that carry orbital angular momentum (OAM) and exhibit a singularity point where the intensity is zero and the phase is undetermined. The OV phase structure can be described mathematically by $\exp(i\ell\theta)$, where θ is the azimuthal coordinate, and the integer ℓ is the so-called azimuthal mode number and is directly related to the topological charge (TC) [1]. Optical vortices have found many applications such as optical tweezers and spanners [2], super resolution spectroscopy [3], light-matter wave interactions in Bose-Einstein condensates [4, 5], communication technologies [6] and nano-fabrication [7, 8].

Interaction of OV beams with nonlinear crystals has been studied in the context of parametric frequency conversion processes [9]. Previous experiments demonstrated that the TC of OV beams can exhibit nondestructive conversion during parametric interactions. By using an OV to pump a mid-infrared optical parametric oscillator, Miyamoto *et al* showed that the TC of the pump laser is selectively transferred to the signal outputs [10]. Optical vortex beams interacting via degenerate two-wave mixing in a Kerr-like nonlinear medium has been investigated experimentally and showed that vortex mixing occurs inside the nonlinear medium, which leads to exchange of topological charge and cascaded generation of vortex beams [11]. Second-harmonic generation (SHG) with vortex beams has also been investigated for two decades; it was found that each mode becomes doubled in frequency and transformed into a higher order vortex mode [12]. Recently, SHG of fractionally-charged OV beams has been studied with femtosecond radiation [13]. The OAM of the generated second harmonic field is always zero and is independent on the displacement of the spiral phase plate which is used to generate the OV beam. How femtosecond OV beams interact within a Raman crystal has not yet been fully explored. This is an interesting subject in that femtosecond OVs is a relatively new area [14–16].

#193113 - $15.00 USD Received 1 Jul 2013; revised 5 Sep 2013; accepted 9 Sep 2013; published 5 Nov 2013

We wish to extend upon our previous work by studying the interaction of femtosecond OVs in a Raman active crystal with the goal of spatio-temporally engineering subcycle optical pulses [17–19]. We have studied coherent transfer of OAM in multi-order Raman sidebands [20] using a pair of linearly chirped pulses (hundreds of femtoseconds in duration), which allowed us to excite the Raman mode at 320 cm^{-1}. However, because this is a coherent process, the output beams are chirped, and a compensator is required to achieve subcycle pulses [21]. One method to overcome this difficulty is to use a two-colored femtosecond scheme employing an OPA. In addition, by using a pair of femtosecond pumping laser pulses from an OPA, we can efficiently access the high gain, high frequency Raman mode of $PbWO_4$ at 901 cm^{-1}. In our earlier experiment, our pump and Stokes beams had either the same charge $\ell_p = \ell_S = |\ell|$ or opposite charges $\ell_p = -\ell_s = |\ell|$ with $|\ell| = 1$. In the current work, we shape each beam independently with the pump and Stokes beam having TCs of $|\ell| = 1$ and 0 respectively. This is an interesting situation because it has been predicted by theoretical calculations that the resulting OVs generated in a Raman medium will have incremental increases of charge 1 from one Raman sideband to the next according to the relationship $\ell_n = \ell_p + n(\ell_p - \ell_s)$. The pairwise sum of the TCs in the n^{th} order AS and S is equal to the sum of the TCs in the pump and Stokes, i.e. $\ell_p + \ell_s = \ell_n + \ell_{-(n+1)}$ [20, 22]. For example, when $\ell_p = 1,\ \ell_s = 0, \text{for}\, n = 5$, the mode number of AS5 is $\ell_5 = 6$ and for S5, the mode number is $\ell_{-6} = -5$. When coherently super-imposing the OVs both spatially and temporally, helical beams can be formed, which allow us to verify another case of the OAM algebra [20, 22].

2. Experimental setup

The experimental setup is shown in Fig. 1. We used a Ti:sapphire amplifier, which outputs 40 fs pulses with center wavelength at 806 nm and having a 1 kHz repetition rate. Part of the beam was used as the pump beam for Raman generation while the other part was used to pump an optical parametric amplifier (OPA). The second harmonic (870 nm) of the idler beam from the OPA was used as the Stokes beam (Here we follow the coherent anti-Stokes Raman scattering convention and denote the shorter 806 nm wavelength beam as pump and the long wavelength 870 nm as the Stokes beam.). We label the sidebands as anti-Stokes one (AS1), anti-Stokes two (AS2), and so on. A typical spectrum and frequency resolved optical gating (FROG) measurement of a single sideband generated in the coherent Raman process had also been shown in Fig. 1 (The sideband is generated in diamond). This showed that, in principle, using femtosecond pulses, we could generate the coherent sidebands in the femtosecond region [21, 23]. In order to perform interferometric experiments, both the pump and the Stokes beams were split into two so that a reference set of Raman sideband could be generated in a 0.5 mm thick Raman crystal $PbWO_4$ (shown as the solid and dotted lines in Fig. 1). The solid-lined pair was used to generate the femtosecond OVs in the Raman sidebands. The pump beam, shaped by a spiral phase plate having an azimuthal structure divided into 16 segments with each step contributing nπ/8 phase shift [24], contained an OV of $\ell = \pm 1$. The other pair of beams (dotted line) was used to generate the reference sidebands with Gaussian profile $\ell_n = 0$. The power of each pump beam is around 5 mW and the power of each Stokes is around 0.5 mW. The power of AS1 is around 0.5 mW. In theory, the center wavelength of the sidebands could be determined by $\omega_n = \omega_p + n\omega_R$, where ω_R is the angular frequency of the Raman mode and ω_n is the center angular frequency of the Raman sideband. In experiments, the frequency spacing between the sidebands decreases gradually for the higher sidebands [17, 25]. Three translation stages were used to control the relative delay

#193113 - $15.00 USD Received 1 Jul 2013; revised 5 Sep 2013; accepted 9 Sep 2013; published 5 Nov 2013

between the pump and Stokes beams of each pair, and to add an overall delay between the reference and OV sidebands. More details can be found in the latter part of this paper.

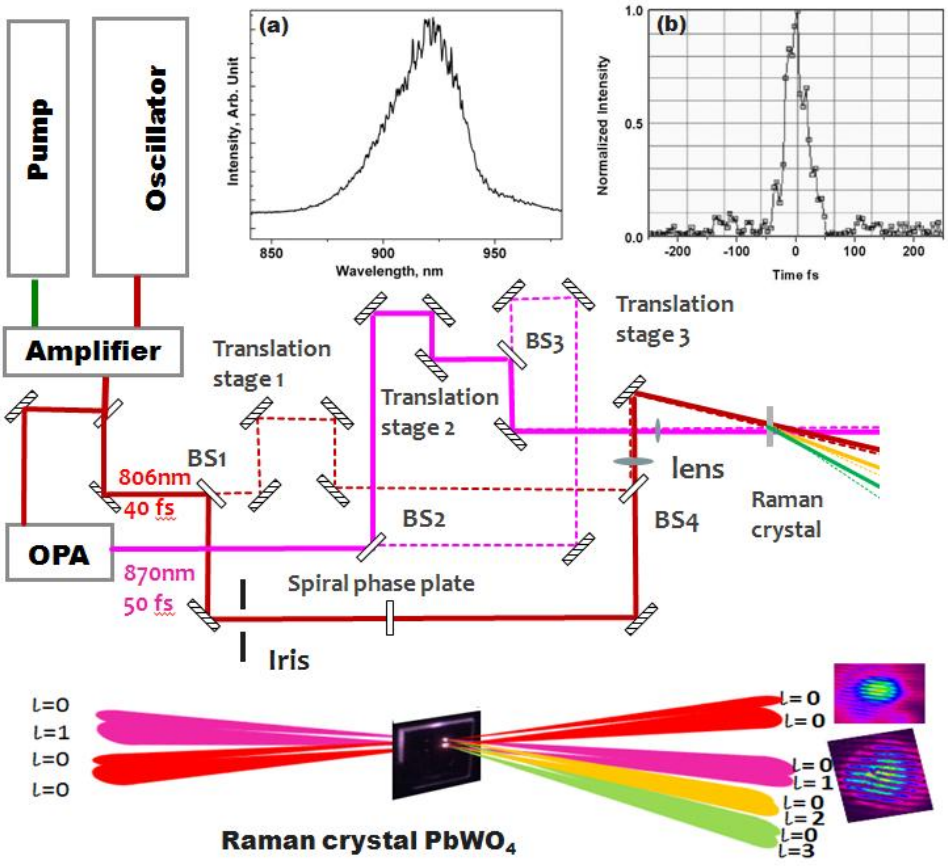

Fig. 1. Schematics of the experiment layout. Two pairs of beams are focused in different part of a Raman-active crystal—PbWO4. The beams are close and overlap partially. The interference of the beams occurs and gives the phase profiles of the optical vortices. The insets (a) and (b) are the typical spectrum and FROG measurement of AS1 generated from Raman crystal (diamond), performed using Phazzler (FastLite). The center wavelength of AS 1 is at 940 nm. The dispersion of the pulse has been corrected by Phazzler. The full-width-half-maximum (FWHM) is measured to be 32.8 fs.

3. Femtosecond optical vortex generation in a $PbWO_4$ Raman-active crystal

In our previous experiments, we focused mainly on the coherent transfer of optical OAM to the sidebands from the pump and Stokes beams [20]. This transfer was observed in the first three orders and was in agreement with predictions. In order to investigate this transfer into the higher orders, improvements to the beam quality were needed. For this reason, we

#193113 - $15.00 USD Received 1 Jul 2013; revised 5 Sep 2013; accepted 9 Sep 2013; published 5 Nov 2013

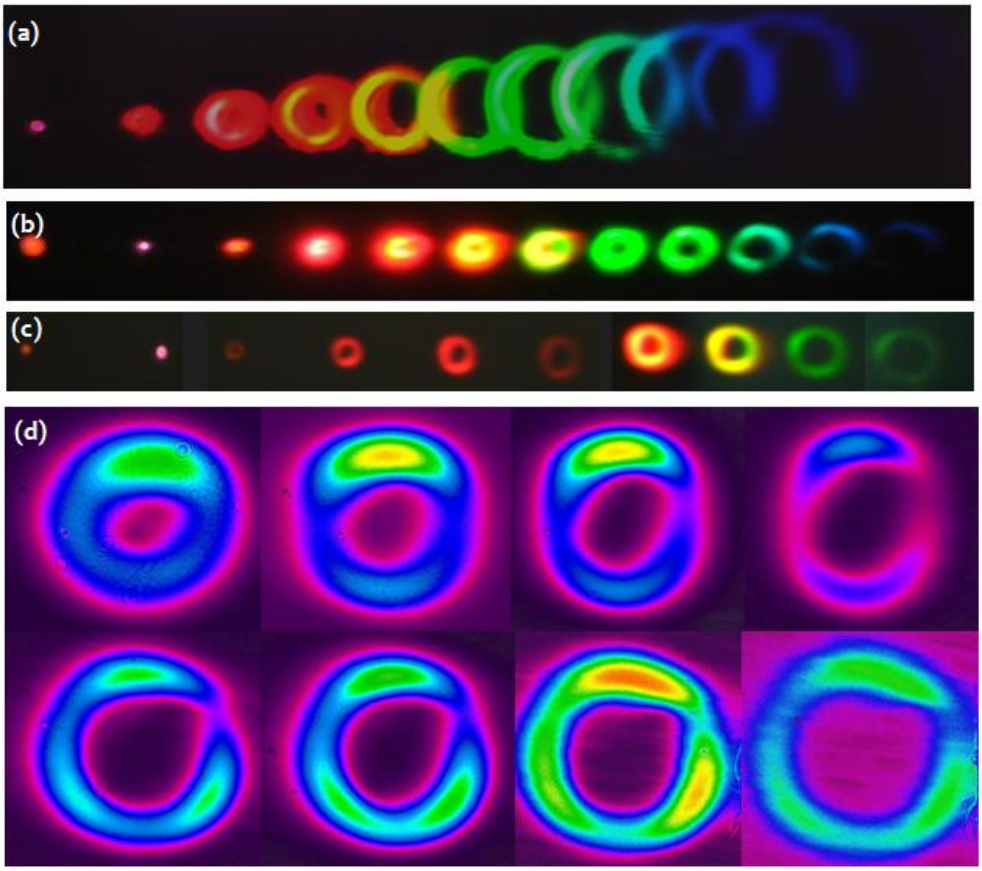

Fig. 2. Different diameter of OVs generated in a Raman crystal by controlling the intensity and the beam diameter. (a): OVs are overlapped because the divergence of OV is bigger than the separation angle between two sidebands. (b): Decreasing the beam waist with iris before SPP to reduce the divergence. OVs are separated. (c): Adjusting the power of pump and Stokes. When the intensity of the pump and Stokes beams are attenuated, low-order sidebands OVs have symmetric beam profiles; OV are ready to be measured. All pictures were taken with a digital camera. (d): The top are beam profiles AS1 to AS4 and the bottom are beam profiles of AS5 to AS8.

explored ways to produce high quality OV beams in the sidebands. For all experiments, the input beams had a few mW of power and were focused by a lens with a nominal focal length of 30 cm. The angle between the pump and Stokes beams was about 4 degrees so that phase matching conditions could be satisfied. This is important as we have shown that phase matching plays an important role in broadband light generation using solids [17]. In order to produce high fidelity ultrashort optical vortices in the sidebands and to accurately measure TCs, high fidelity input OV beams are necessary. For this reason, The SPP was adjusted until highly symmetric doughnut-shaped beams were produced. In addition, much care was taken to align the temporal and spatial overlaps, and to adjust the relative size of the pump and Stokes beams.

#193113 - $15.00 USD Received 1 Jul 2013; revised 5 Sep 2013; accepted 9 Sep 2013; published 5 Nov 2013

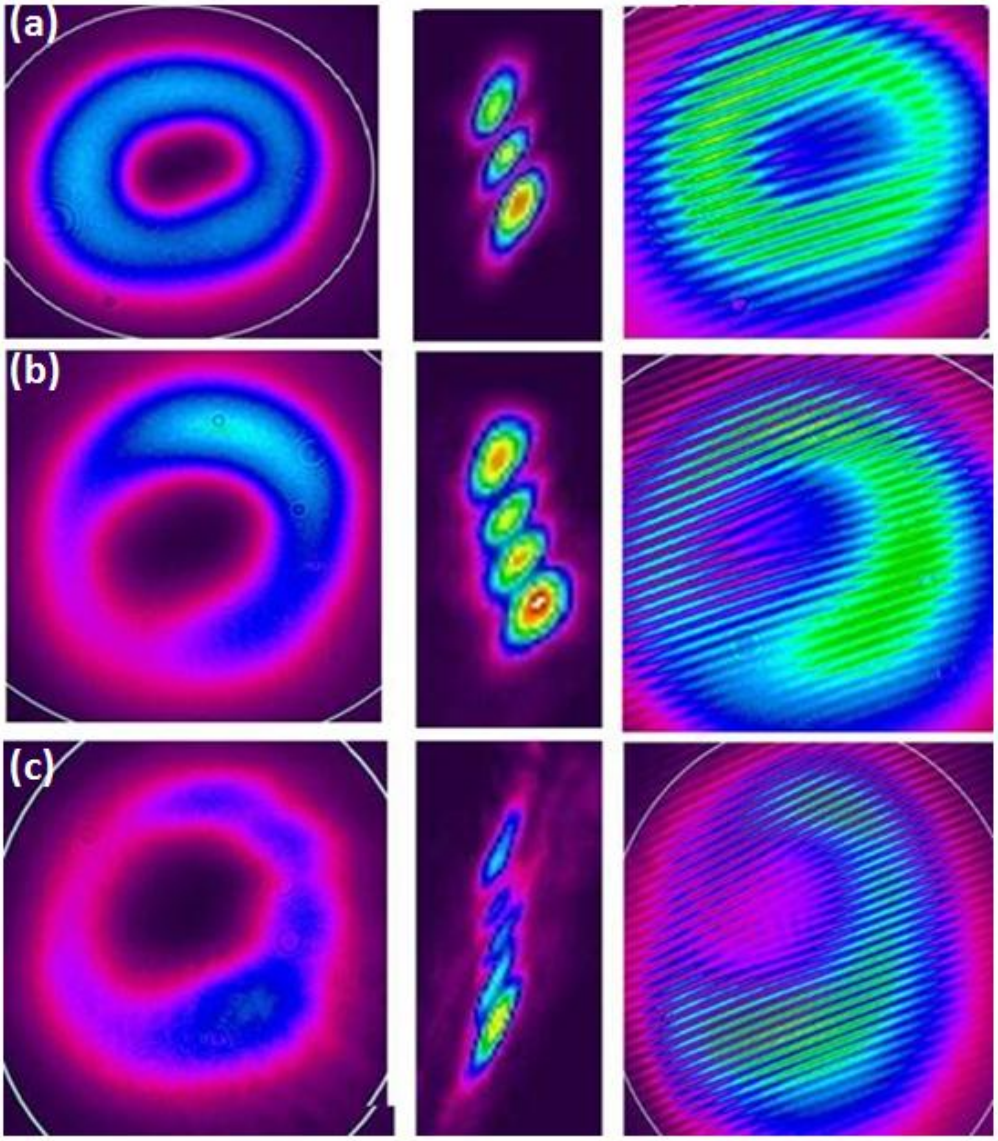

Fig. 3. OV sidebands topological charge measurement using a tilted lens. Row a (b, c), AS1 (2, 3) are the OVs before the lens, after the lens and interference with a Gaussian reference beam.

The results of our first experiment are shown in Fig. 2(a). Up to 8 ring-shaped sidebands were observed, however, these sidebands overlap making it impossible to independently manipulate their phases/amplitudes or measure the TC. Because the divergence of Laguerre Gaussian beams depends inversely on the beam waist $\theta \sim \lambda / w_0$ and because the waist is inversely related to the beams size w_L at the lens $w_0 \sim \lambda f / w_L$, the divergence of the beams are proportional to the beams size at the lens $\theta \sim w_L / f$. Therefore, to separate the OV sidebands, we controlled their divergence by adjusting the iris before the lens in our setup. Figure 2(b) shows the result of the separate OV beams up to the tenth order as a consequence of reducing their divergence angle.

Pulse energy is another important factor, and it must be managed because higher pulse energies lead to nonlinear effects such as self-focusing resulting in sideband distorted. To

#193113 - $15.00 USD Received 1 Jul 2013; revised 5 Sep 2013; accepted 9 Sep 2013; published 5 Nov 2013

demonstrate this, we show an images of OVs generated at different power levels. The maximum power of each pump beam is around 5 mW. The intensity for the pump beam on the crystal is around 10^{11} W/cm^2. The maximum power of the Stokes beam is around 0.5 mW. The intensity for the Stokes beam on the crystal is around 10^{10} W/cm^2. The OVs Fig. 2(a) and Fig. 2(b) were generated with more pulse energy. The OVs displayed in Fig. 2(c) were measured at a decreased beam power. Although only a few sideband OVs are generated, the intensity is more uniform across the rings than those shown in Fig. 2(a) and (b) taken at higher pulse energies.

4. Topological charge measurement

Various methods have been proposed to measure the topological charge of OVs such as annular and triangular apertures [26, 27]. Here we first measure the TC of our Raman sidebands by a simple method which has been recently proposed —a tilted convex lens [28]. By tilting a lens to a tangent angle of about 6 degrees and recording the intensity distribution of a propagating vortex at the focus, the sign and magnitude of the OV can be determined. As

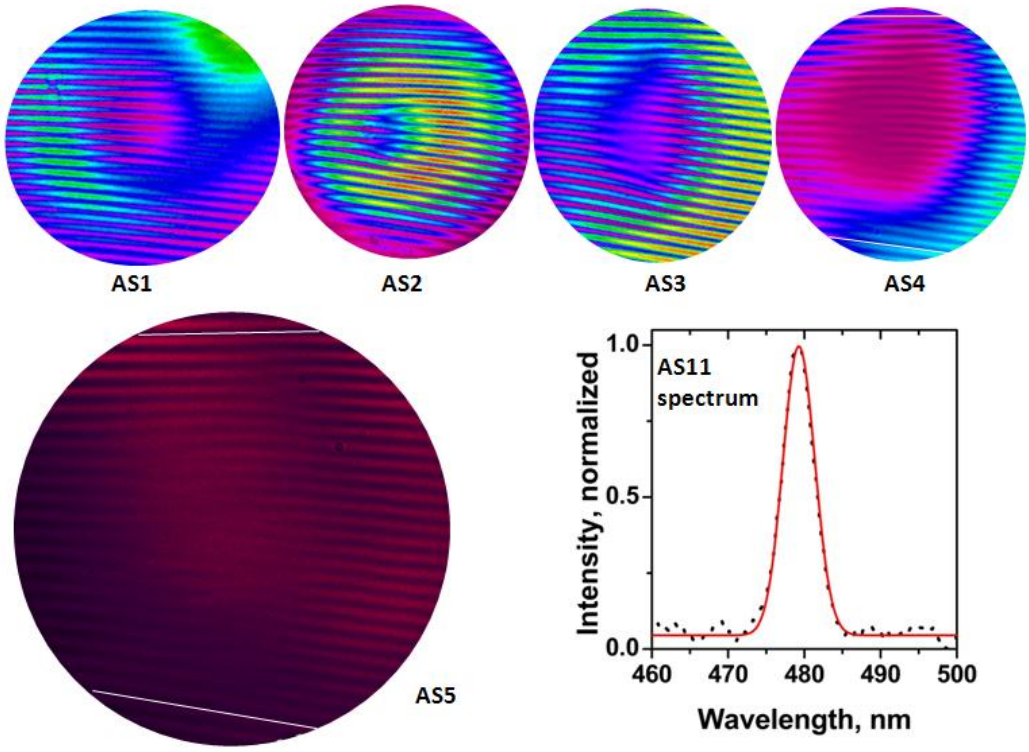

Fig. 4. Interference patterns of the Raman sidebands orders AS1 to AS5. We also show the spectrum of the AS11 OV (black dotted line) with a Gaussian spectrum (red line) fit that is centered on 479nm. This spectral profile is Gaussian, and is capable of supporting a Fourier-transform-limited pulse duration of 68 fs.

an example, we can measure the TC by counting the nodes of the beam profiles at the focus shown in the middle column of Fig. 3. We used low power for the pump and Stokes beams so that only a few sidebands were generated, which corresponds to the low power situation in Fig. 2. The results of the OV charge measurements are shown in Fig. 3.

This method does give a quick check of the TC of the sidebands; however, to obtain detailed phase information, we find that the interferometer is the best method [20]. To this

#193113 - $15.00 USD Received 1 Jul 2013; revised 5 Sep 2013; accepted 9 Sep 2013; published 5 Nov 2013

end, we have split the pump and Stokes beams into two. The first pair of beams (solid lines in Fig. 1) has relatively more power and was focused on the bottom bright spot on the crystal, while the second pair was focused on the top spot on the crystal, as shown schematically in Fig. 1. As mentioned above, the pump beam in the first pair was shaped by a spiral phase plate and had a TC of 1. When the pump and Stokes in each pair of beams were spatially and temporally overlapped, we realized generation of many order of Raman sidebands. By adjusting the temporal delay between the two pairs of beams, Young's interference experiment was simultaneously realized for each sideband. These OV-containing sidebands have a larger diameter and were partially overlapped with the sidebands that were generated by the Gaussian reference pair. The interference between the two sets of sidebands is used to determine the helicity and topological charge in each order. In Fig. 1, we show the common straight fringe pattern for the Stokes beam, which has OAM of 0, and a typical fork pattern, which results from the interference of two pump beams with ℓ = 0 and 1 respectively. We have found that the OAM is transferred to the higher anti-Stokes orders according to $\ell_n = \ell_p + n(\ell_p - \ell_s)$. By using interference, the TCs of the anti-Stokes (AS) Raman sidebands were measured up to 3 orders for low power pumps, as shown in Fig. 3. The interference fringes of the Raman sideband orders up to AS3 are consistent with that expected from the OAM algebra. To observe the interference of AS4 and AS5 orders, more pump and Stokes pulse energy was needed. In Fig. 4, we show the AS1 to AS5 OV sidebands charge measurements using slightly higher powers of the pump beams. The interference pattern of the AS orders AS1—AS3 are similar to the low power situation although the OV shapes become slightly distorted (less symmetric) possibly due to other nonlinear processes such as self-focusing. For high-order sideband such as AS4 and AS5 we used higher pulse energies in addition to an iris which was used to cut the high intensity ring and focus on the dark core region (Fig. 4). In between the two white lines on the interference phase map of AS4, there are 20 bright fringes on the left side and 25 on the right side. This indicates that the TC is 5. Similarly for AS4, on the left there are 20 constructive interference fringes while on the right side there are 26, which give the measurement TC of 6.

Instead of the expected general multifurcation for TC of order $\ell > 1$, where the singularity is at a single point, we observed splitting of the multifurcation into several smaller multifurcations when both low and high energy pump and Stokes pulses were used. The sums of the bifurcations/multifurcations will give us the mode number ℓ_n. When we moved the beam profiler along the beam propagation direction of the beams we observed stable fringes. We therefore concluded that this splitting occurs with high-energy femtosecond pulses, and we suspected that the splitting may have occurred inside the Raman crystal following generation. This is highly probable as it is well-known that high order vortices $|\ell| > 1$ are unstable and split into several charge 1 vortices [29]. We speculate that by using a thinner crystal, we may be able to avoid such splitting and further increase the fidelity of these beams. Although we are not able to measure the topological charge of the sidebands beyond AS5, the donut-like sidebands can be seen up to 8th order with increasing diameter (Fig. 2 (a) and (b)). This increase is an indication of the presence of high-order OAM [20].

5. Summary

In conclusion, we have generated many orders of multi-color OV beams by focusing an OAM containing pump beam and a femtosecond Stokes beams into a Raman-active crystals. We have shown that the OVs are sensitive to the pulse energy, beam diameter as well as the spatial-temporal overlaps of the beam. We used two methods—a tilted lens and an interferometer to measure the TC of the OVs and found that the generated OVs follow OAM transfer in a way similar to frequency conversion. The interference fringes of the OV beams and Gaussian reference beam show that the high-order OVs generated inside Raman crystals are unstable and split in to several charge 1 OVs. In a previous experiment using a nearly

#193113 - $15.00 USD Received 1 Jul 2013; revised 5 Sep 2013; accepted 9 Sep 2013; published 5 Nov 2013

identical setup, we measured the coherent Raman sidebands generated in diamond [21, 23]. This previous work showed that with the assistance of a pulse shaper and prism, we could synthesize ultrafast waveform using the first five Raman sidebands covering the spectral range from 752 nm to 580 nm. These vortices, in principle, could support a 3.5 fs vortex beam, if spatially and temporally combined with proper phases.

Acknowledgments

This work is supported by the National Science Foundation (grants PHY-1307153, No. 0722800, and 1058510) and Robert A. Welch Foundation (grants A1546 and A1547).

#193113 - $15.00 USD Received 1 Jul 2013; revised 5 Sep 2013; accepted 9 Sep 2013; published 5 Nov 2013